Title

Azide—Alkyne Click Conjugation on Quantum Dots by Selective Copper Coordination

Journal

ACS Nano, 12(5)

ISSN

1936-0851

Authors

Mann, Victor R

Powers, Alexander S

Tilley, Drew C

et al.

Publication Date

2018-05-22

DOI

10.1021/acsnano.8b00575

Peer reviewed

HHS Public Access

Author manuscript

ACS Nano. Author manuscript; available in PMC 2018 May 23.

Published in final edited form as:

ACS Nano. 2018 May 22; 12(5): 4469–4477. doi:10.1021/acsnano.8b00575.

Azide–Alkyne Click Conjugation on Quantum Dots by Selective Copper Coordination

Victor R. Mann[†,#], **Alexander S. Powers**[†], **Drew C. Tilley**[‡], **Jon T. Sack**[‡], and **Bruce E. Cohen**[*,†]

[†]The Molecular Foundry, Lawrence Berkeley National Laboratory, Berkeley, California 94720, United States

[#]Department of Chemistry, University of California, Berkeley, California 94720, United States

[‡]Department of Physiology and Membrane Biology, University of California, Davis, California 95616, United States

Abstract

Functionalization of nanocrystals is essential for their practical application, but synthesis on nanocrystal surfaces is limited by incompatibilities with certain key reagents. The copper-catalyzed azide-alkyne cycloaddition (CuAAC) is among the most useful methods for ligating molecules to surfaces, but has been largely useless for semiconductor quantum dots (QDs) because Cu^+ ions quickly and irreversibly quench QD fluorescence. To discover non-quenching synthetic conditions for Cu-catalyzed click reactions on QD surfaces, we developed a combinatorial fluorescence assay to screen >2000 reaction conditions to maximize cycloaddition efficiency while minimizing QD quenching. We identify conditions for complete coupling without significant quenching, which are compatible with common QD polymer surfaces and various azide/alkyne pairs. Based on insight from the combinatorial screen and mechanistic studies of Cu coordination and quenching, we find that superstoichiometric concentrations of Cu can promote full coupling if accompanied by ligands that selectively compete the Cu from the QD surface but allow it to remain catalytically active. Applied to the conjugation of a K^+ channel-specific peptidyl toxin to CdSe/ZnS QDs, we synthesize unquenched QD conjugates and image their specific and voltage-dependent affinity for K^+ channels in live cells.

Keywords

quantum dot; CuAAC; quenching; copper; synthesis; combinatorial nanoscience; bioconjugation; high-throughput screen

[*]Corresponding Author: becohen@lbl.gov.

Author Contributions

The manuscript was written through contributions of all authors. All authors have given approval to the final version of the manuscript.

Competing Financial Interests

The authors declare no competing financial interests.

Supporting Information. The following files are available free of charge *via* the internet at http://pubs.acs.org.

Supplementary methods; tables of reagents, reagent structures, correlation analysis; reaction schemes; molecular modeling; figures with quenching and combinatorial screen analysis for various reaction parameters (PDF)

Optical microscopy is the primary means of studying complex living systems, enabling real-time analysis of individual cellular components at high spatial and temporal resolution. Semiconductor quantum dot (QD) nanocrystals are outstanding probes for light microscopy, with exceptionally high photostability, large optical cross-sections, large Stokes shifts, and demonstrated uses in multiplexed and single molecule experiments.[1–3] Like other hydrophobic nanocrystals, QDs must be transferred to water and their surfaces functionalized to have any utility as imaging probes or biosensors.[4–5] While a number of bioconjugation reactions have been adapted for QDs,[6–9] others have been found to destroy the exceptional optical properties of the nanocrystal.[10–11] Broadening the scope of QD surface conjugation chemistry is essential to expand the reach of QDs for imaging applications.

In the development of optical sensors of neuronal activity, we sought a method to conjugate QDs (Figure 1a) to the peptidyl tarantula toxin guangxitoxin-1E (GxTX), a 36-amino acid cystine knot peptide that binds Kv2 channel voltage sensing domains (Figure S1),[12] which we have previously synthesized to contain propargylglycine alkyne sidechains for chemoselective bioconjugation.[13] The Cu-catalyzed azide-alkyne 1,3-dipolar click coupling (CuAAC) is among the most widely used reactions for both bioconjugation[14–16] and for modification of surfaces.[17–18] CuAAC reactions are bioorthogonal, work well in dilute aqueous conditions, and require only a Cu ion catalyst and mild reducing agent to form covalent bonds between terminal alkynes and azides.[19–21] However, Cu ions have been found to be exceptionally strong and irreversible quenchers of QD fluorescence, even with brief exposures at nanomolar concentrations (Figure 1c).[7, 11, 22–23] Previous work has shown that Cu^{+} is primarily responsible for QD quenching[7] and that large (>10 nm) and heavily crosslinked polymer networks are required to prevent Cu from reaching the nanocrystal surface.[24–25] It is not clear whether this quenching is due to rapid Cu/Cd exchange[26] or the Cu ions are acting as proximal electron traps, but in our initial experiments we observed no change in QD emission wavelength maximum or lineshape following Cu exposure (Figure 1d). Our attempts to reverse Cu quenching by exposure to high affinity Cu ligands or excess Cd^{2+} were unsuccessful, even after extended incubations (Figure S2). While copper-free azide-alkyne coupling methods have been successful in eliminating copper toxicity from this reaction on cells[27–28], the necessary strained alkynes are of limited use in certain complex structures such as 3-cystine knot peptides.[13] Here, we report a 2000-reaction combinatorial FRET-based assay to screen for suppression of fast Cu quenching of QDs while maintaining Cu catalytic activity. Based on insight from this screen and mechanistic studies of Cu coordination and quenching, we find that superstoichiometric concentrations of Cu can promote full coupling if accompanied by ligands that selectively compete the Cu from the QD surface but allow it to remain catalytically active. With these conditions, we synthesize unquenched peptidyl toxin-QD conjugates and image their specific and state-dependent affinity for K^{+} channels in live mammalian cells.

RESULTS AND DISCUSSION

Screening for non-quenching CuAAC reaction conditions

We anticipated that the amphiphilic polymer coatings commonly used to passivate QDs in water[29–31] would offer a low-dielectric layer inhospitable to Cu ions, but initial CuAAC reactions with azide-bearing QDs showed only rapid quenching with no apparent conjugation (Figure 1). Addition of a series of Cu-coordinating ligands (Table S1) that have been shown to accelerate CuAAC cycloadditions[32–35] did not measurably prevent quenching unless also completely preventing the cycloaddition. Given this poor initial reactivity, the complexity of the CuAAC mechanism,[21, 36–39] and the number of components and concentrations that can be varied, we sought a high-throughput approach to screen for synthetic conditions that might create a Cu complex able to catalyze CuAAC cycloaddition but unable to interact directly with the nanocrystal. Previous FRET-based synthetic screens have been successful in discovery of catalysts and in improving the efficiencies of coupling reactions, including Cu^{+}-mediated CuAAC couplings.[40–44] While these screens have focused on maximizing coupling efficiencies, we faced the added challenge of optimizing the relatively slow Cu^{+}-mediated coupling reaction in the presence of the rapid Cu^{+}-mediated quenching of nanocrystal fluorescence. For this screen, we synthesized an alkynyl cyanine compound as a fluorescent acceptor paired with aqueous azide-coated CdSe/CdS core/shell QDs with emission maxima at 625 nm and 90% quantum yield (Figure 2a, and Methods). Based on previous mechanistic[21, 36–39] and empirical studies of CuAAC optimization,[33, 45] we selected a series of parameters to vary, including Cu source, alkyne/azide stoichiometry, reducing agent concentration, Cu-coordinating ligands,[32–34] other counterions (in the form of buffer anions), and reaction time (Tables S1 and S2). Initial tests showed strong effects on both CuAAC coupling and quenching (Figure 2), as seen in the appearance Cy5 acceptor emission and maintenance of QD emission beyond the ~10 s that would be required for full quenching under standard CuAAC conditions (Figure 1c).

To expand the reach of the combinatorial screen, we carried out reactions in 96-well plates and measured spectra by plate reader. At specified time points, reactions were quenched by dilution into 10 mM EDTA solutions, and a full emission spectrum collected for each well. In a typical experiment, 8 reactions testing a single parameter were halted at 11 different time points to generate a 2-dimensional reaction series. A compilation of ~1200 such reactions (Figure 3a), plotting integrated QD intensity *versus* integrated Cy5 intensity, shows a small fraction of reaction conditions with strong emission at both wavelengths. To determine the maximal FRET efficiency for this system, we synthesized fully Cy5-ligated QDs using a parallel Cu-free reaction on these same QDs by first reducing the azides to amines and then coupling with Cy5 succinimidyl esters (Scheme S1). These QDs show no reactivity with alkynes through CuAAC coupling but do undergo efficient reaction with activated esters (Figure S3). Comparison of this emission (Figure 3a, black star) with the combinatorial Cu-mediated reactions, several conclusions are readily apparent. All points closest to the maximal FRET emission are at acidic pH (Figures 2b and 3a), suggestive of a surprising pH dependence. Reaction times >5 min are clustered near the axes, indicative of strong QD quenching (x-axis), minimal CuAAC coupling (y-axis), or loss of acceptor signal due to quenching of the QD donor. Low acceptor emission may arise from QD quenching,

little CuAAC activity, or both. While such conditions are useless as preparative synthetic conditions, they do highlight the need to find reaction conditions that enable complete CuAAC on unusually fast timescales.

Analysis of combinatorial screening data

To quantify which variables have the strongest effects on QD quenching and CuAAC coupling, we analyzed this spectral data for pairwise correlations between each parameter and either QD or Cy5 emission (Figures 3d–e and Table S3). The strongest effect on QD quenching is the dependence on reaction pH, with little measured quenching below pH 4 to full and rapid quenching above pH 8. Acceptor emission is largely indifferent to reaction pH, suggesting differences between Cu quenching and catalysis that can be leveraged to optimize non-quenching CuAAC couplings. Changes to Cu-coordinating ligand concentration did not significantly affect either reaction (Figures 3d–e), but we did observe major differences depending on the chemistry of the Cu coordination (Figure 2e and Table S1). Strong chelators (*e.g.*, cysteine) prevented quenching but also prevented any measurable CuAAC coupling, suggesting charged ligands can prevent Cu^{+} from reaching the nanocrystal surface but may also inhibit interaction with the alkyne.[21, 36–37] Two triazole-based ligands (THPTA and BTTAA) proved most effective at generating Cy5 FRET emission while ameliorating quenching (Table S1), and optimization with THPTA gave us a FRET spectrum most similar to that of the QD-Cy5 conjugate synthesized without Cu (Figure 3b). Previous work has shown that BTTAA is superior to other Cu ligands for promoting CuAAC coupling with hydrophobic substrates,[33, 45–46] while in this case the QD surfaces and Cy5 are both hydrophilic, possibly explaining the differences seen here.

Mechanisms of Cu-mediated cycloaddition and quenching

To understand the results of the FRET screen, we examined the reactivity of other azide and alkyne compounds, as well as other amphiphilic polymer coatings. Changing the azide inorganic nanocrystal shell from CdS to ZnS had no significant effect (Figure S4), but conditions for passivating QDs with amphiphilic polymer proved critical, with added surfactant (*e.g.*, oleic acid) in the hydrophobic QD dispersion essential for preparing aqueous QDs resistant to Cu quenching by diffusion to the nanocrystal surface (Figure 4). Changing the azide from nanocrystal to the organic fluorophore Cy3 (Scheme S2) led to higher optimal pH and longer reaction times (Figure S5). This suggests the low pH optimal for QD CuAAC is needed to slow quenching but has no significant effects on the cycloaddition, corroborating analysis from the pairwise variable analysis (Figure 3d–e). The optimal Cy3-Cy5 CuAAC conditions square well with previous findings for small molecule coupling,[14, 44] while differences with the QD-Cy5 conditions suggest reaction conditions unique for QD substrates.

One explanation for these differences is that the polyacrylic acid-derived polymer passivating the QD (see ref 31 and Methods) concentrates Cu ions at the poly-carboxylate surface (Figure 4), close enough to CuAAC substrates to speed the reaction by more than an order of magnitude compared to small molecule CuAAC. This may also explain the pH dependence, in which low pH causes increased turnover of Cu ions from surface carboxylates. Another surprising finding of the screen is that a full equivalent of Cu (50 μM)

or more is required for CuAAC with the QD, but not the organic fluorophore (Figure S5). This suggests a certain fraction of the Cu is either unable to react, because it is coordinated to QD surface carboxylates, or to turn over, because Cu release from the substrate is slow until the reaction is quenched by a large excess of EDTA (Figure 4). Indeed, we found that allowing reactions to incubate in EDTA solution for extended periods typically led to increases in acceptor emission, although without full restoration of QD emission (Figure S6). This suggests that Cu ions are bound to the QD surface even after initial addition of EDTA, and some are bound very tightly, possibly in or on the inorganic nanocrystal.

To test whether Cu bound to the nanoparticle surface is responsible for QD quenching during CuAAC reactions, we included a series of benign divalent metal ions (*i.e.*, Ca^{2+}, Mg^{2+}, Mn^{2+}) in the reaction mixture in addition to Cu and Cu ligands. These added ions have been shown to neither quench QDs[11, 47] nor interfere with CuAAC reactions,[46, 48] but in these reactions, all reduced quenching and increased CuAAC coupling (Figure S7). In addition, using common passivation polymers where the number of surface carboxylates can be varied (poly(maleic anhydride-*alt*-octadecene); [49] Figure 1b and Scheme S3), we found that the rate of quenching decreases as the number of surface carboxylates decreases, while still allowing for the CuAAC coupling to occur (Figure S7). Compared to the PAOA surface polymer used in the high-throughput screen (Figure 3), for this polymer, higher Cu:QD stoichiometries are tolerated before QD quenching is observed (Figure S8). Superstoichiometric quantities of Cu do not quench QDs only with an appropriate excess of triazole THPTA ligand (Figure S8), suggesting a complex competition for Cu between QD surface carboxylates, the triazole ligand, the QD surface, and the alkyne (Figure 4). Tuning the ratios of Cu to triazole and alkyne yields both high coupling and low quenching, and this phenomenon is transferable across surface passivation polymers (Figure S9). In contrast to most previous studies of CuAAC conditions,[15, 19, 34, 38] we find a 10-fold molar equivalent of Cu over the azide is most efficient (Figure S8), allowing for rapid (<2 min) reactions before QD quenching begins to become apparent. Our combinatorial approach also offers a large dataset to be mined for insight into aqueous CuAAC reactions and other mechanistic questions (Figures S10–S12).

Cu-mediated click synthesis of QD bioconjugates

To test the relevance of these non-quenching CuAAC conditions to complex biomolecules, we coupled azide-bearing CdSe/CdS QDs with the tarantula toxin GxTX, an amphiphilic 36-amino acid cysteine knot peptide.[12–13] GxTX selectively binds to membrane-embedded voltage sensors of Kv2 channels in the resting state (Figure S1), and can be released by membrane depolarization.[13] We synthesized and refolded Ser13Pra GxTX, where the alkyne sidechain is predicted to extend into extracellular solution[12] and used CuAAC conditions from the combinatorial screen for conjugation. The reaction was limited to 90 s to limit the number of GxTX per QD (Figure S13) and minimize non-specific membrane staining. CHO cells with and without induced channel expression were incubated with QD-GxTX conjugates and imaged along with a cellular autofluorescence band outside of the QD emission (Figure 5). Cells with high levels of Kv2.1 expression show significant increases in membrane QD staining compared to cells with low Kv2.1 expression, or to cells stained with unconjugated QDs (Figure 5g). Membrane depolarization induced by the addition of high [K

$^{+}]_o$ solution decreases membrane staining to background levels (Figure 5e–f), demonstrating that binding is dependent on the conformational state of the channel and the QD-conjugated GxTX remains physiologically active. Because of their sensitivity to changes in membrane potential, these conjugates are a first generation QD-based voltage sensor, whose sensitivity and optical properties may be refined through choice of nanoparticle and toxin.

CONCLUSIONS

We have discovered rapid, non-destructive, and high-yield CuAAC reaction conditions with Cu^{+} concentrations that would normally fully quench QD emission in under 10 s. Compared to previous synthetic screens, the added challenge of maintaining catalysis while suppressing a faster side-reaction is apparent in the size of the screens: about 2000 reactions in this study *versus* 100–200 in most others.[40–44] Some important discoveries from the screen include pH dependence of QD quenching, the superiority of triazole Cu ligands for QD coupling, and the advantages for superstoichiometric concentrations of Cu. These synthetic conditions are applicable to other molecules containing simple alkynes, including peptides, oligonucleotides, lipids, and carbohydrates,[20] as well as to other imaging probes prone to Cu quenching, such as lanthanide-doped nanocrystals.[50–51] This work demonstrates a combinatorial approach for adapting otherwise incompatible reactions to quantum dots, suggesting a more expansive view of organic synthetic possibilities on nanocrystal surfaces.

MATERIALS AND METHODS

Synthesis of CdSe/CdS core/shell quantum dots

Quantum dots were synthesized as reported[2, 31] and characterized by TEM, DLS, UV-visible absorption, and fluorescence emission. See Supporting Information for full synthetic details.

Passivation of Core-shell CdSe/CdS Nanoparticles by poly(acrylic acid)-*co*-poly(*n*-octylacrylamide)-*co*-poly(2-aminoethylacrylamide) (PAOA) amphiphilic copolymer

CdSe/CdS QD core/shells with emission maxima of 626 nm were dispersed in hexane with 1% (*v*/*v*) oleic acid to 8 μM,; CdSe/ZnS QD core/shells (Ocean Nanotech) with emission maxima of 585 nm were diluted with hexane to 5 μM. Concentrations were determined by first exciton absorbance. For aqueous dispersion, PAOA (20 mg, 6.25 μmol, 3000-fold molar excess over QDs) was dissolved in 1 mL of MeOH and 19 mL of $CHCl_3$. QDs in hexane (*e.g.*, 250 μL of 8 μM 626 nm CdSe/CdS QDs, 2.0 nmol) were added with stirring, and the solvents were removed under a gentle stream of N_2 overnight. The dry QD/polymer residue was then resuspended in 15 mL of 200 mM sodium bicarbonate buffer, pH 8.0. This suspension was sonicated for 30 minutes, heated in an 80 °C water bath for 60 minutes, slowly cooled in the bath to room temperature, and then sonicated for 30 minutes. Excess polymer was removed by spin dialysis (Amicon Ultra-15, 50 kDa MWCO), washing with 3 × 15 mL of 100mM HEPES, pH 7.8. The retentate was diluted to 1 mL with HEPES buffer and centrifuged at 16100 × *g* for 5 min to remove residual polymer and insoluble aggregates. Aqueous QD dispersions were stored under ambient conditions.

Passivation of QDs by poly(maleic anhydride-*alt*-1-octadecene) (PMAO) amphiphilic copolymer

PMAO (30 mg, 1.33 μmol, 16 monomer units per nm^2 of QD surface) was dissolved in 1 mL of acetone and 14 mL of $CHCl_3$. QDs in hexane (*e.g.*, 250 μL of 8 μM 626 nm CdSe/CdS QDs, 2.0 nmol) were added with stirring, and the solvents were evaporated under a gentle stream of N_2 overnight. The QD/polymer residue was then resuspended in 15 mL of 50 mM sodium borate buffer, pH 9.0, with desired ratios of primary amines for reaction with maleic anhydrides (Scheme S3). This suspension was sonicated for 30 minutes, heated in an 80 °C water bath for 60 minutes, slowly cooled in the bath to room temperature, and then sonicated for 30 minutes. Excess polymer was removed by spin dialysis (Amicon Ultra-15, 50 kDa MWCO), washing with 3 × 15 mL of 100 mM HEPES, pH 7.8. The retentate was diluted to 1 mL with HEPES buffer and centrifuged at 16100 × *g* for 5 min to remove residual polymer and insoluble aggregates. Aqueous QDs were further purified by size exclusion chromatography (HiPrep 16/60 Sephacryl S-500HR, GE Healthcare), and aqueous QD dispersions were stored under ambient conditions.

Synthesis of azide-coated QDs

PAOA-wrapped QDs (2 μM, 1 mL) in 100 mM HEPES, pH 7.8, and SE-PEG_4-N_3 (ThermoFisher, 50 mM in DMSO, 100 μL) in DMSO were combined in a 1.5-mL centrifuge tube and shaken for 1 hour on a rotary mixer. The reaction mixture was diluted to 500 μL with Milli-Q water, and excess PEG reagent was removed by spin dialysis (50 kDa MWCO), washing with 3 × 500 μL of Milli-Q water. The retentate was diluted to 1 mL with Milli-Q water and stored under ambient conditions.

Synthesis of PEG_4-amino coated QDs

Azide-coated QDs (2 μM, 100 μL) were mixed with sodium borohydride (100 mM, 100 μL) in 100 mM sodium bicarbonate buffer, pH 10.0, and stirred in a vented glass vial for 2 hours. The reaction was ended and remaining borohydride destroyed by addition of 2 mL of 100 mM phosphate buffer, pH 4.5, followed by stirring for 30 minutes. The reaction mixture was diluted to 500 μL with 100 mM HEPES, pH 7.8, and the QDs were purified by spin dialysis (50 kDa MWCO), washing with 3 × 500 μL of HEPES buffer. The retentate was diluted to 100 μL with HEPES buffer and stored under ambient conditions.

Synthesis of Cy5-alkyne

Propargylamine (0.8 μL, 12.5 μmol) was dissolved in 400 μL of 100 mM HEPES pH 7.4, which was added to 1 mg of dry Cy5 succinimidyl ester (1.26 μmol, GE Healthcare). The reaction was vortexed well, briefly centrifuged, and incubated overnight in the dark. The alkyne product was purified on a C_{18} HPLC column (Vydac) using a linear 2–60% CH_3CN gradient with 0.1% TFA over 30 min, with product eluting at 21 min (28% CH_3CN). MS, $C_{36}H_{44}N_3O_7S_2$ $(MH)^+$ calculated: 694.25; found: 694.8. Fractions containing product were pooled and lyophilized to 0.83 mg (94% yield) of dark blue film.

Syntheses of Texas Red-alkyne and Alexa Fluor 594-alkyne were performed under similar conditions and eluted at 49% and 37% CH_3CN respectively. MS, Texas Red-alkyne,

$C_{40}H_{45}N_4O_7S_2$ $(MH)^+$ calculated: 757.27; found: 757.5; Alexa Fluor 594-alkyne, $C_{38}H_{38}N_3O_{10}S_2$ $(MH)^+$ calculated: 760.18; found: 760.4.

Synthesis of Cy3-Azide

1-Amino-11-azido-3,6,9-trioxaundecane (0.8 μL, 4.0 μmol, Sigma) was dissolved in 20 μL of 200mM sodium bicarbonate pH 8.2, which was added to dry Cy3 succinimidyl ester (150 μg, 196 nmol, GE Healthcare). The reaction was vortexed well, briefly centrifuged, and incubated overnight in the dark. The azide product was purified on a C_{18} HPLC column (Vydac) using a linear 2–60% CH_3CN gradient with 0.1% TFA over 30 min, with product eluting at 18 min (22% CH_3CN). MS, $C_{39}H_{54}N_6O_{10}S_2$ M^- calculated: 829.33; found: 829.5. Fractions containing product were pooled and lyophilized to 0.13 mg (79% yield) of dark pink film.

Cu-QD quenching and reversal

Emission spectra were measured on a Fluoromax fluorometer (Horiba Jobin Yvon) from 10 nM dispersions of PAOA-encapsulated CdSe/CdS QDs with 405 nm excitation. A solution of $Cu(OAc)_2$ and sodium ascorbate was quickly mixed into the QDs to give final concentrations of 10 μM and 20 μM, respectively. Emission at 625 nm was measured at 1-s intervals for 2000 s, and full emission spectra were recorded both before and after the kinetic experiment. For reversal tests, ligands were added to a final concentration of 10 mM, with or without 1 mM $CdCl_2$. Emission at 625 nm was measured at 5-min intervals for 30 h, with full emission spectra recorded both before and after the kinetic experiment.

Combinatorial CuAAC FRET assay

In a typical reaction, two reagent mixtures were prepared prior to reaction initiation in the following order: Tube A: 40 μL of 2 μM QD-PEG-N_3 (0.08 nmol), 12 μL of 350 μM Cy5-alkyne (4.2 nmol), and 10 μL of 50 mM phosphate-citrate buffer, pH 4.5. Tube B: 8 μL of 500 μM $CuSO_4$ (4 nmol), 8 μL of 50 mM sodium ascorbate (400 nmol), and 2 μL of 20 mM THPTA (40 nmol) in Milli-Q water. Solution B was rapidly mixed into Solution A, and time points were taken 1, 2, 3, 4, 5, 7, 10, 15, 20, and 30 min after mixing, by removing 7-μL aliquots and adding into 350 μL of 10 mM EDTA solution in wells of a black wall 96-well assay plate. Fluorescence spectra were measured in a SpectraMax Gemini EM fluorescence plate reader (Molecular Devices) with 405 nm excitation and recorded with a 1-nm step size from 550 – 750 nm. Each reaction series contained an internal standard of unmodified QDs for concentration scaling. Spectra on key samples were also collected in cuvets in a fluorometer.

Data analysis

Reaction parameters and corresponding spectral data were imported into JMP (SAS Institute, Inc.) for data manipulation and statistical analysis. All trials were scaled to QD concentration prior to cross-parameter comparisons. Each scaled spectrum was integrated from 600 – 630 nm for the QD emission value and from 670 – 700 nm for the Cy5 emission value. The Pearson product-moment correlation coefficient and its significance were calculated for each reaction parameter paired with both the QD emission and Cy5 emission

to determine the influence of each variable.[52–54] Coefficients near zero show no dependence between variables, and values near ±1 indicate highly correlated responses to changes in the parameters. The reaction from each ligand type that displayed maximum FRET signal was scaled for concentration, and a difference spectrum was generated by subtraction of the unmodified QD signal. The 670 – 700 nm integrated emission from the difference peak was used as a relative measure of maximum ligand efficacy (Table S1).

Non-quenching CuAAC reaction conditions on QDs

For reactions at acidic pH: aqueous QDs (2 μM, 40 μL) were mixed with 12 μL of 350 μM alkyne and 10 μL of 80 mM phosphate-citrate buffer pH 4.5. In a separate tube, 8 μL of 5 mM $CuSO_4$, 8 μL of 50 mM sodium ascorbate, and 2 μL of 100 mM THPTA were mixed well and added to the first tube with rapid mixing. After 2 minutes, the reaction was quenched into 400 μL of 10 mM EDTA solution.

For reactions at physiological pH: aqueous QDs (2 μM, 40 μL) were mixed with 12 μL of 350 μM alkyne, 2 μL 100 mM $Ca(NO_3)_2$ or $MgSO_4$, and 8 μL of 100 mM HEPES buffer pH 7.4. In a separate tube, 8 μL of 2.5 mM $CuSO_4$, 8 μL of 50 mM sodium ascorbate, and 2 μL of 50 mM THPTA were mixed well and added to the first tube with rapid mixing. After 30 seconds, the reaction was quenched into 400 μL of 10 mM EDTA solution.

Reactions may be purified by spin dialysis, washing with 500 μL of 20 mM HEPES, pH 7.4, containing 500 μM EDTA, and then with 3 × 500 μL of 20 mM HEPES, pH 7.4. Yields of both reactions are estimated to be >90% based on fluorescence measurements in comparison to control QD conjugates.

Synthesis of QD-GxTX conjugates

Alkyne-bearing guangxitoxin-1E mutants were synthesized as previously described.[13] Two reagent mixtures were prepared prior to reaction initiation in the following order: Tube A: 40 μL of 2 μM QD-PEG-N_3 (0.08 nmoles), 2 μL of 2.3 mM Ser13Pra GxTX (4.6 nmoles) in 50% DMSO, 10 μL of Milli-Q water, and 10 μL of 50 mM phosphate-citrate buffer pH 4.5. Tube B: 8 μL of 500 μM $CuSO_4$ (4 nmoles), 8 μL of 50 mM sodium ascorbate (400 nmoles), and 2 μL of 20 mM THPTA (40 nmoles) in Milli-Q water. Tube B was rapidly mixed into tube A, allowed to react for 90 s, and then quenched in 400 μL of 10 mM EDTA. QD-GxTX conjugates were purified by spin dialysis (50 kDa MWCO, Amicon), washing with 500 μL of 20 mM HEPES, pH 7.4, containing 500 μM EDTA, and then with 3 × 500 μL of 20 mM HEPES, pH 7.4. The retentate was diluted to 160 μL with HEPES buffer and stored under ambient conditions.

Cell Culture

CHO-K1 cells were maintained in tissue culture-treated polystyrene dishes (Nunc) at 37 °C in a 5% CO_2 atmosphere in Ham's F-12 media (Sigma) containing 10% fetal bovine serum (FBS, Gibco) and 1% penicillin–streptomycin solution (Life Technologies). A CHO-K1 cell line expressing rat Kv2.1 voltage-gated potassium channels[13] was cultured with 1 μg/mL blasticidin (ThermoFisher) and 25 μg/mL zeocin (Invitrogen) to retain transfected vectors.

Before experiments, 1 μg/mL minocycline was added to the cell media 2 days prior to imaging to induce Kv2.1 expression.

Live Cell Imaging

Cells were plated in 8-chamber culture slides (Ibidi) 2 days prior to imaging experiments and imaged in neuronal external solution (NES; concentration in mM: 3.5 KCl, 135 NaCl, 1.5 $CaCl_2$, 1 $MgCl_2$, 10 HEPES, pH 7.4 with NaOH). Cells were incubated in freshly prepared 5 nM QD-GxTX or 5 nM QD-PAOA in NES for 20 minutes on ice to prevent endocytosis of nanoparticles, and then washed with 3 × 400 μL of NES immediately prior to imaging under ambient conditions. Confocal images of the focal plane at the chamber interface were obtained using an inverted Zeiss LSM710 system with a 1.4 N.A. 63x Apochromat oil immersion objective. QD emission was excited using a 405 nm diode laser with an MBS-445 main dichroic beam splitter, and emission was collected from 560 – 610 nm. Cellular autofluorescence was excited with the same 405 nm diode laser with an MBS-405 main dichroic beam splitter, and emission was collected from 450 – 500 nm. To increase K^+ concentration for cell depolarization, NES was aspirated from the wells and replaced with NES containing 135 mM KCl and 3.5 mM NaCl. High-[K^+] images in Figure 5 were taken 5 minutes after NES replacement. Regions of interest (ROI) were manually drawn around 100 cells from a single well for each imaging category. Total integrated pixel intensity was calculated for both 560 – 610 nm QD fluorescence and 450 – 500 nm autofluorescence, and a ratio of the two was calculated within each ROI. The data were pooled for each imaging category and a Student's t-test was used to determine statistical differences in mean intensity ratios for each category (Figure 5). All cell imaging and statistics shown were taken in the same imaging session with the same reagents. Similar results were obtained for 3 separate experiments with different batches of cells and GxTX-QDs. Images and analysis in Figure 5 are for cells at >80% confluence coinciding with GxTX-QDs synthesized within the prior 24 h.

Molecular Docking

The model of GxTx-1E—Kv1.2-Kv2.1 chimera complex was performed using ROSETTA as described previously.[12] Briefly, the voltage sensor of a Kv1.2-Kv2.1 channel (PDB 2R9R)[55] was docked with a GxTx-1E NMR structure (PDB 2WH9).[56] After energy minimization, the lowest energy binding model most consistent with alanine scan mutagenesis was selected for rendering. Molecular renderings were produced using the UCSF Chimera package from the Computer Graphics Laboratory, University of California, San Francisco.

Supplementary Material

Refer to Web version on PubMed Central for supplementary material.

Acknowledgments

We thank Y. Liu for a generous supply of BTTAA, E. Chan and S. Fletcher-Taylor for discussion, and R. Zuckermann for comments on the manuscript. This work was supported by CAL-BRAIN award 350327 (B.E.C.) and National Institutes of Health award R01NS096317 (B.E.C. and J.T.S.). Work at the Molecular Foundry was supported by the Director, Office of Science, Office of Basic Energy Sciences, Division of Materials Sciences and Engineering, of the U.S. Department of Energy under Contract No. DE-AC02-05CH11231.

References

1. Medintz IL, Uyeda HT, Goldman ER, Mattoussi H. Quantum Dot Bioconjugates for Imaging, Labelling and Sensing. Nat Mater. 2005; 4:435–446. [PubMed: 15928695]
2. Chen O, Zhao J, Chauhan VP, Cui J, Wong C, Harris DK, Wei H, Han HS, Fukumura D, Jain RK, Bawendi MG. Compact High-Quality CdSe-CdS Core-Shell Nanocrystals with Narrow Emission Linewidths and Suppressed Blinking. Nat Mater. 2013; 12:445–451. [PubMed: 23377294]
3. Boles MA, Ling D, Hyeon T, Talapin DV. The Surface Science of Nanocrystals. Nat Mater. 2016; 15:141–153. [PubMed: 26796733]
4. Hildebrandt N, Spillmann CM, Algar WR, Pons T, Stewart MH, Oh E, Susumu K, Daz Sa, Delehanty JB, Medintz IL. Energy Transfer with Semiconductor Quantum Dot Bioconjugates: A Versatile Platform for Biosensing, Energy Harvesting, and Other Developing Applications. Chem Rev. 2017; 117:536–711. [PubMed: 27359326]
5. Bilan R, Fleury F, Nabiev I, Sukhanova A. Quantum Dot Surface Chemistry and Functionalization for Cell Targeting and Imaging. Bioconjugate Chem. 2015; 26:609–624.
6. Clapp AR, Medintz IL, Mauro JM, Fisher BR, Bawendi MG, Mattoussi H. Fluorescence Resonance Energy Transfer between Quantum Dot Donors and Dye-Labeled Protein Acceptors. J Am Chem Soc. 2004; 126:301–310. [PubMed: 14709096]
7. Han HS, Devaraj NK, Lee J, Hilderbrand SA, Weissleder R, Bawendi MG. Development of a Bioorthogonal and Highly Efficient Conjugation Method for Quantum Dots Using Tetrazine-Norbornene Cycloaddition. J Am Chem Soc. 2010; 132:7838–7839. [PubMed: 20481508]
8. Goldman ER, Balighian ED, Mattoussi H, Kuno MK, Mauro JM, Tran PT, Anderson GP. Avidin: A Natural Bridge for Quantum Dot-Antibody Conjugates. J Am Chem Soc. 2002; 124:6378–6382. [PubMed: 12033868]
9. Sun D, Gang O. DNA-Functionalized Quantum Dots: Fabrication, Structural, and Physicochemical Properties. Langmuir. 2013; 29:7038–7046. [PubMed: 23706124]
10. Shen H, Jawaid AM, Snee PT. Poly(Ethylene Glycol) Carbodiimide Coupling Reagents for the Biological and Chemical Functionalization of Water-Soluble Nanoparticles. ACS Nano. 2009; 3:915–923. [PubMed: 19275175]
11. Ao ZC, Zheng GU, Eng J-lZ, Iu J-hL, Eng QD, An J-bF, Iang J-nX. A Novel Fluorescent Probe for Copper Ions Based on Polymer-Modified Cdse Cds Core Shell Quantum Dots. Anal Sci. 2011; 27:643–647. [PubMed: 21666363]
12. Gupta K, Zamanian M, Bae C, Milescu M, Krepkiy D, Tilley DC, Sack JT, Yarov-Yarovoy V, Kim JI, Swartz KJ. Tarantula Toxins Use Common Surfaces for Interacting with Kv and ASIC Ion Channels. elife. 2015; 4:e06774. [PubMed: 25948544]
13. Tilley DC, Eum KS, Fletcher-Taylor S, Austin DC, Dupre C, Patron LA, Garcia RL, Lam K, Yarov-Yarovoy V, Cohen BE, Sack JT. Chemoselective Tarantula Toxins Report Voltage Activation of Wild-Type Ion Channels in Live Cells. Proc Natl Acad Sci U S A. 2014; 111:E4789–E4796. [PubMed: 25331865]
14. Hong V, Presolski SI, Ma C, Finn MG. Analysis and Optimization of Copper-Catalyzed Azide-Alkyne Cycloaddition for Bioconjugation. Angew Chem Int Ed Engl. 2009; 48:9879–9883. [PubMed: 19943299]
15. Lallana E, Riguera R, Fernandez-Megia E. Reliable and Efficient Procedures for the Conjugation of Biomolecules through Huisgen Azide-Alkyne Cycloadditions. Angew Chem Int Ed Engl. 2011; 50:8794–8804. [PubMed: 21905176]
16. Uttamapinant C, Tangpeerachaikul A, Grecian S, Clarke S, Singh U, Slade P, Gee KR, Ting AY. Fast, Cell-Compatible Click Chemistry with Copper-Chelating Azides for Biomolecular Labeling. Angew Chem Int Ed Engl. 2012; 51:5852–5856. [PubMed: 22555882]
17. White MA, Johnson JA, Koberstein JT, Turro NJ. Toward the Syntheses of Universal Ligands for Metal Oxide Surfaces: Controlling Surface Functionality through Click Chemistry. J Am Chem Soc. 2006; 128:11356–11357. [PubMed: 16939250]
18. Boisselier E, Salmon L, Ruiz J, Astruc D. How to Very Efficiently Functionalize Gold Nanoparticles by “Click” Chemistry. Chem Commun (Cambridge, U K). 2008:5788–5790.

19. Rostovtsev VV, Green LG, Fokin VV, Sharpless KB. A Stepwise Huisgen Cycloaddition Process: Copper(I)-Catalyzed Regioselective "Ligation" of Azides and Terminal Alkynes. Angew Chem Int Ed Engl. 2002; 41:2596–2599. [PubMed: 12203546]
20. Lutz JF, Zarafshani Z. Efficient Construction of Therapeutics, Bioconjugates, Biomaterials and Bioactive Surfaces Using Azide-Alkyne "Click" Chemistry. Adv Drug Deliv Rev. 2008; 60:958–970. [PubMed: 18406491]
21. Berg R, Straub BF. Advancements in the Mechanistic Understanding of the Copper-Catalyzed Azide-Alkyne Cycloaddition. Beilstein J Org Chem. 2013; 9:2715–2750. [PubMed: 24367437]
22. Callan JF, Mulrooney RC. Luminescent Detection of Cu(Ii) Ions in Aqueous Solution Using Cdse and Cdse-Zns Quantum Dots Functionalised with Mercaptosuccinic Acid. Phys Status Solidi C. 2009; 6:920–923.
23. Beaune G, Tamang S, Bernardin A, Bayle-Guillemaud P, Fenel D, Schoehn G, Vinet F, Reiss P, Texier I. Luminescence of Polyethylene Glycol Coated Cdsete/Zns and Inp/Zns Nanoparticles in the Presence of Copper Cations. Chemphyschem. 2011; 12:2247–2254. [PubMed: 21661091]
24. Merkl JP, Wolter C, Flessau S, Schmidtke C, Ostermann J, Feld A, Mews A, Weller H. Investigations of Ion Transport through Nanoscale Polymer Membranes by Fluorescence Quenching of Cdse/Cds Quantum Dot/Quantum Rods. Nanoscale. 2016; 8:7402–7407. [PubMed: 26987974]
25. Ostermann J, Merkl JP, Flessau S, Wolter C, Kornowksi A, Schmidtke C, Pietsch A, Kloust H, Feld A, Weller H. Controlling the Physical and Biological Properties of Highly Fluorescent Aqueous Quantum Dots Using Block Copolymers of Different Size and Shape. ACS Nano. 2013; 7:9156–9167. [PubMed: 24032605]
26. Li H, Zanella M, Genovese A, Povia M, Falqui A, Giannini C, Manna L. Sequential Cation Exchange in Nanocrystals: Preservation of Crystal Phase and Formation of Metastable Phases. Nano Lett. 2011; 11:4964–4970. [PubMed: 21961554]
27. Jewett JC, Bertozzi CR. Cu-Free Click Cycloaddition Reactions in Chemical Biology. Chem Soc Rev. 2010; 39:1272–1279. [PubMed: 20349533]
28. Agard NJ, Prescher JA, Bertozzi CR. A Strain-Promoted [3 + 2] Azide-Alkyne Cycloaddition for Covalent Modification of Biomolecules in Living Systems. J Am Chem Soc. 2004; 126:15046–15047. [PubMed: 15547999]
29. Pellegrino T, Manna L, Kudera S, Liedl T, Koktysh D, Rogach AL, Keller S, Radler J, Natile G, Parak WJ. Hydrophobic Nanocrystals Coated with an Amphiphilic Polymer Shell: A General Route to Water Soluble Nanocrystals. Nano Lett. 2004; 4:703–707.
30. Albers AE, Chan EM, McBride PM, Ajo-Franklin CM, Cohen BE, Helms BA. Dual-Emitting Quantum Dot/Quantum Rod-Based Nanothermometers with Enhanced Response and Sensitivity in Live Cells. J Am Chem Soc. 2012; 134:9565–9568. [PubMed: 22642769]
31. Wichner SM, Mann VR, Powers AS, Segal MA, Mir M, Bandaria JN, DeWitt MA, Darzacq X, Yildiz A, Cohen BE. Covalent Protein Labeling and Improved Single-Molecule Optical Properties of Aqueous Cdse/Cds Quantum Dots. ACS Nano. 2017; 11:6773–6781. [PubMed: 28618223]
32. Presolski SI, Hong V, Cho SH, Finn MG. Tailored Ligand Acceleration of the Cu-Catalyzed Azide-Alkyne Cycloaddition Reaction: Practical and Mechanistic Implications. J Am Chem Soc. 2010; 132:14570–14576. [PubMed: 20863116]
33. Wang W, Hong S, Tran A, Jiang H, Triano R, Liu Y, Chen X, Wu P. Sulfated Ligands for the Copper(I)-Catalyzed Azide-Alkyne Cycloaddition. Chem - Asian J. 2011; 6:2796–2802. [PubMed: 21905231]
34. Rodionov VO, Presolski SI, Diaz DD, Fokin VV, Finn MG. Ligand-Accelerated Cu-Catalyzed Azide-Alkyne Cycloaddition: A Mechanistic Report. J Am Chem Soc. 2007; 129:12705–12712. [PubMed: 17914817]
35. Rodionov VO, Presolski SI, Gardinier S, Lim YH, Finn MG. Benzimidazole and Related Ligands for Cu-Catalyzed Azide-Alkyne Cycloaddition. J Am Chem Soc. 2007; 129:12696–12704. [PubMed: 17914816]
36. Worrell BT, Malik JA, Fokin VV. Direct Evidence of a Dinuclear Copper Intermediate in Cu(I)-Catalyzed Azide-Alkyne Cycloadditions. Science. 2013; 340:457–460. [PubMed: 23558174]

37. Zhu L, Brassard CJ, Zhang X, Guha PM, Clark RJ. On the Mechanism of Copper(I)-Catalyzed Azide-Alkyne Cycloaddition. Chem Rec. 2016; 16:1501–1517. [PubMed: 27216993]
38. Kuang GC, Guha PM, Brotherton WS, Simmons JT, Stankee LA, Nguyen BT, Clark RJ, Zhu L. Experimental Investigation on the Mechanism of Chelation-Assisted, Copper(Ii) Acetate-Accelerated Azide-Alkyne Cycloaddition. J Am Chem Soc. 2011; 133:13984–14001. [PubMed: 21809811]
39. Ziegler MS, Lakshmi KV, Tilley TD. Dicopper Cu(I)Cu(I) and Cu(I)Cu(Ii) Complexes in Copper-Catalyzed Azide-Alkyne Cycloaddition. J Am Chem Soc. 2017; 139:5378–5386. [PubMed: 28394586]
40. Stauffer SR, Hartwig JF. Fluorescence Resonance Energy Transfer (Fret) as a High-Throughput Assay for Coupling Reactions. Arylation of Amines as a Case Study. J Am Chem Soc. 2003; 125:6977–6985. [PubMed: 12783551]
41. Scheck RA, Dedeo MT, Iavarone AT, Francis MB. Optimization of a Biomimetic Transamination Reaction. J Am Chem Soc. 2008; 130:11762–11770. [PubMed: 18683929]
42. Finbloom JA, Han K, Slack CC, Furst AL, Francis MB. Cucurbit[6]Uril-Promoted Click Chemistry for Protein Modification. J Am Chem Soc. 2017; 139:9691–9697. [PubMed: 28650616]
43. Kolodych S, Rasolofonjatovo E, Chaumontet M, Nevers MC, Creminon C, Taran F. Discovery of Chemoselective and Biocompatible Reactions Using a High-Throughput Immunoassay Screening. Angew Chem Int Ed Engl. 2013; 52:12056–12060. [PubMed: 24123594]
44. Lewis WG, Magallon FG, Fokin VV, Finn MG. Discovery and Characterization of Catalysts for Azide-Alkyne Cycloaddition by Fluorescence Quenching. J Am Chem Soc. 2004; 126:9152–9153. [PubMed: 15281783]
45. Besanceney-Webler C, Jiang H, Zheng T, Feng L, Soriano del Amo D, Wang W, Klivansky LM, Marlow FL, Liu Y, Wu P. Increasing the Efficacy of Bioorthogonal Click Reactions for Bioconjugation: A Comparative Study. Angew Chem Int Ed Engl. 2011; 50:8051–8056. [PubMed: 21761519]
46. Soriano Del Amo D, Wang W, Jiang H, Besanceney C, Yan AC, Levy M, Liu Y, Marlow FL, Wu P. Biocompatible Copper(I) Catalysts for *in Vivo* Imaging of Glycans. J Am Chem Soc. 2010; 132:16893–16899. [PubMed: 21062072]
47. Prasuhn DE, Feltz A, Blanco-Canosa JB, Susumu K, Stewart MH, Mei BC, Yakovlev AV, Loukov C, Mallet JM, Oheim M, Dawson PE, Medintz IL. Quantum Dot Peptide Biosensors for Monitoring Caspase 3 Proteolysis and Calcium Ions. ACS Nano. 2010; 4:5487–5497. [PubMed: 20822159]
48. Hong V, Steinmetz NF, Manchester M, Finn MG. Labeling Live Cells by Copper-Catalyzed Alkyne--Azide Click Chemistry. Bioconjug Chem. 2010; 21:1912–1916. [PubMed: 20886827]
49. Niculaes D, Lak A, Anyfantis GC, Marras S, Laslett O, Avugadda SK, Cassani M, Serantes D, Hovorka O, Chantrell R, Pellegrino T. Asymmetric Assembling of Iron Oxide Nanocubes for Improving Magnetic Hyperthermia Performance. ACS Nano. 2017; 11:12121–12133. [PubMed: 29155560]
50. Chan EM, Levy ES, Cohen BE. Rationally Designed Energy Transfer in Upconverting Nanoparticles. Adv Mater. 2015; 27:5753–5761. [PubMed: 25809982]
51. Levy ES, Tajon CA, Bischof TS, Iafrati J, Fernandez-Bravo A, Garfield DJ, Chamanzar M, Maharbiz MM, Sohal VS, Schuck PJ, Cohen BE, Chan EM. Energy-Looping Nanoparticles: Harnessing Excited-State Absorption for Deep-Tissue Imaging. ACS Nano. 2016; 10:8423–8433. [PubMed: 27603228]
52. Mansson R, Tsapogas P, Akerlund M, Lagergren A, Gisler R, Sigvardsson M. Pearson Correlation Analysis of Microarray Data Allows for the Identification of Genetic Targets for Early B-Cell Factor. J Biol Chem. 2004; 279:17905–17913. [PubMed: 14960572]
53. Kao KJ, Chang KM, Hsu HC, Huang AT. Correlation of Microarray-Based Breast Cancer Molecular Subtypes and Clinical Outcomes: Implications for Treatment Optimization. BMC Cancer. 2011; 11:143. [PubMed: 21501481]
54. Scheiber J, Jenkins JL, Sukuru SC, Bender A, Mikhailov D, Milik M, Azzaoui K, Whitebread S, Hamon J, Urban L, Glick M, Davies JW. Mapping Adverse Drug Reactions in Chemical Space. J Med Chem. 2009; 52:3103–3107. [PubMed: 19378990]

55. Long SB, Tao X, Campbell EB, MacKinnon R. Atomic Structure of a Voltage-Dependent K+ Channel in a Lipid Membrane-Like Environment. Nature. 2007; 450:376–382. [PubMed: 18004376]

56. Lee S, Milescu M, Jung HH, Lee JY, Bae CH, Lee CW, Kim HH, Swartz KJ, Kim JI. Solution Structure of Gxtx-1e, a High-Affinity Tarantula Toxin Interacting with Voltage Sensors in Kv2. 1 Potassium Channels. Biochemistry. 2010; 49:5134–5142. [PubMed: 20509680]

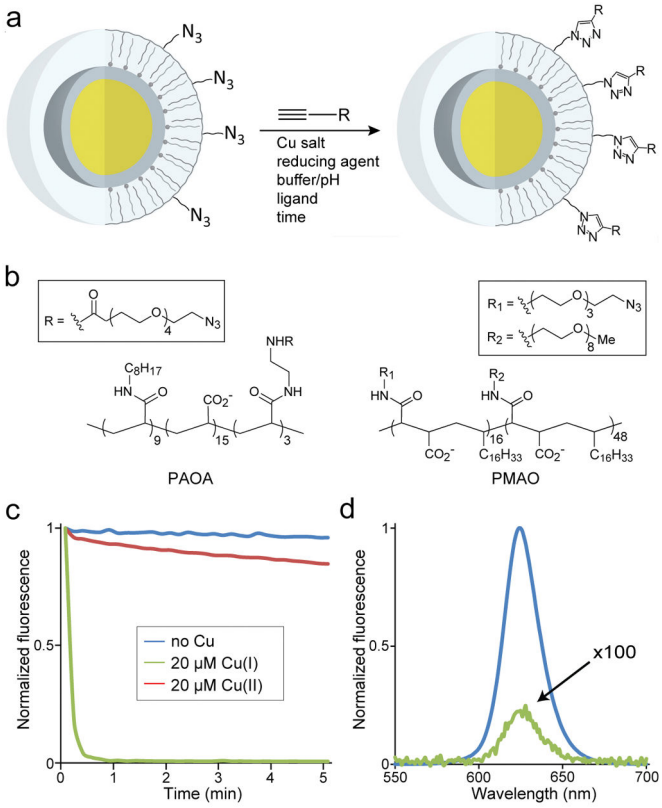

Figure 1.

Copper-mediated click reactions on QD surfaces. (a) CuAAC reaction of alkynes with amphiphilic polymer-coated core/shell QDs, listing reaction variables tested in this study. (b) Structures of surface polymers and azide linkers. (*Left*) Polyacrylic acid-based amphiphilic random co-polymer,[30–31] with azide PEG linker modification. (*Right*) Co-maleic anhydride-octadecene polymer[29, 49] modified with azide PEG linkers and inert PEG amines. Stoichiometries are estimates based on polymer molecular weights, and positions of monomers are random. (c) Kinetic emission of 10 nM QDs with and without exposure to Cu ions. (d) QD emission spectra before (blue) and after (green, shown magnified 100-fold) addition of 20 μM Cu^{+}.

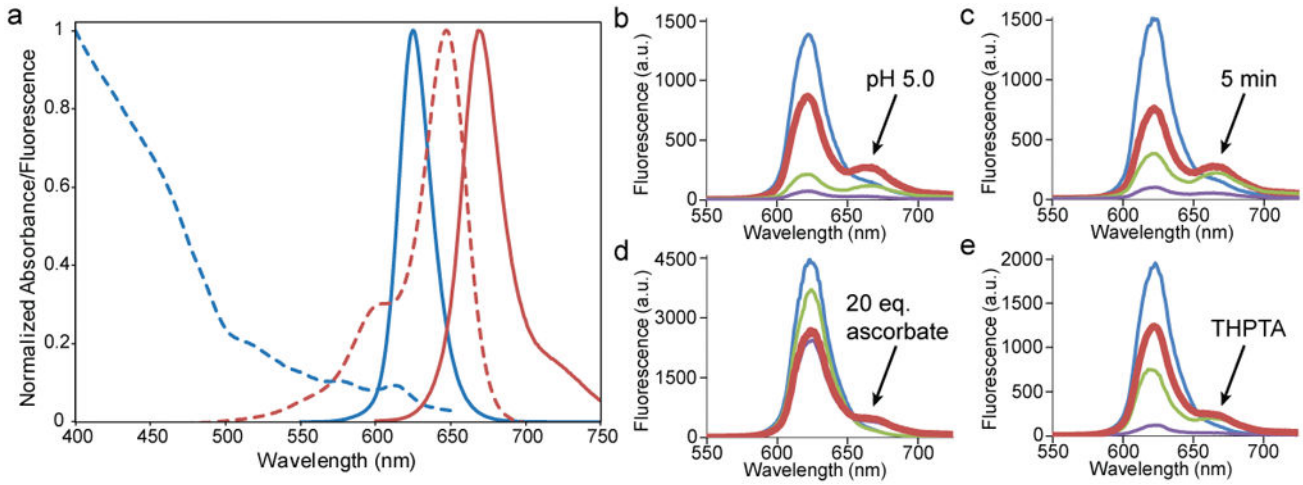

Figure 2.

FRET-based screen for improved CuAAC reaction with minimized QD quenching. (a) Absorbance (dashed) and emission (solid) spectra for CdSe/CdS QD donor (blue) and Cy5 acceptor (red). (b–e) Optimization of FRET emission spectra following 405-nm excitation, for reactions varying: (b) pH: 3.5 (blue), 5.0 (red). 7.5 (green), 9.0 (purple). (c) time (min): 1 (blue), 5 (red). 10 (green), 20 (purple). (d) ascorbate concentration (Cu eq.): 0 (blue), 2 (green). 20 (red), 100 (purple). (e) ligand (all 10 Cu eq.): L-cysteine (blue), THPTA (red), BTTAA (green), L-methionine (purple). See Supplemental Information Methods for full reaction details. Best CuAAC conditions are highlighted.

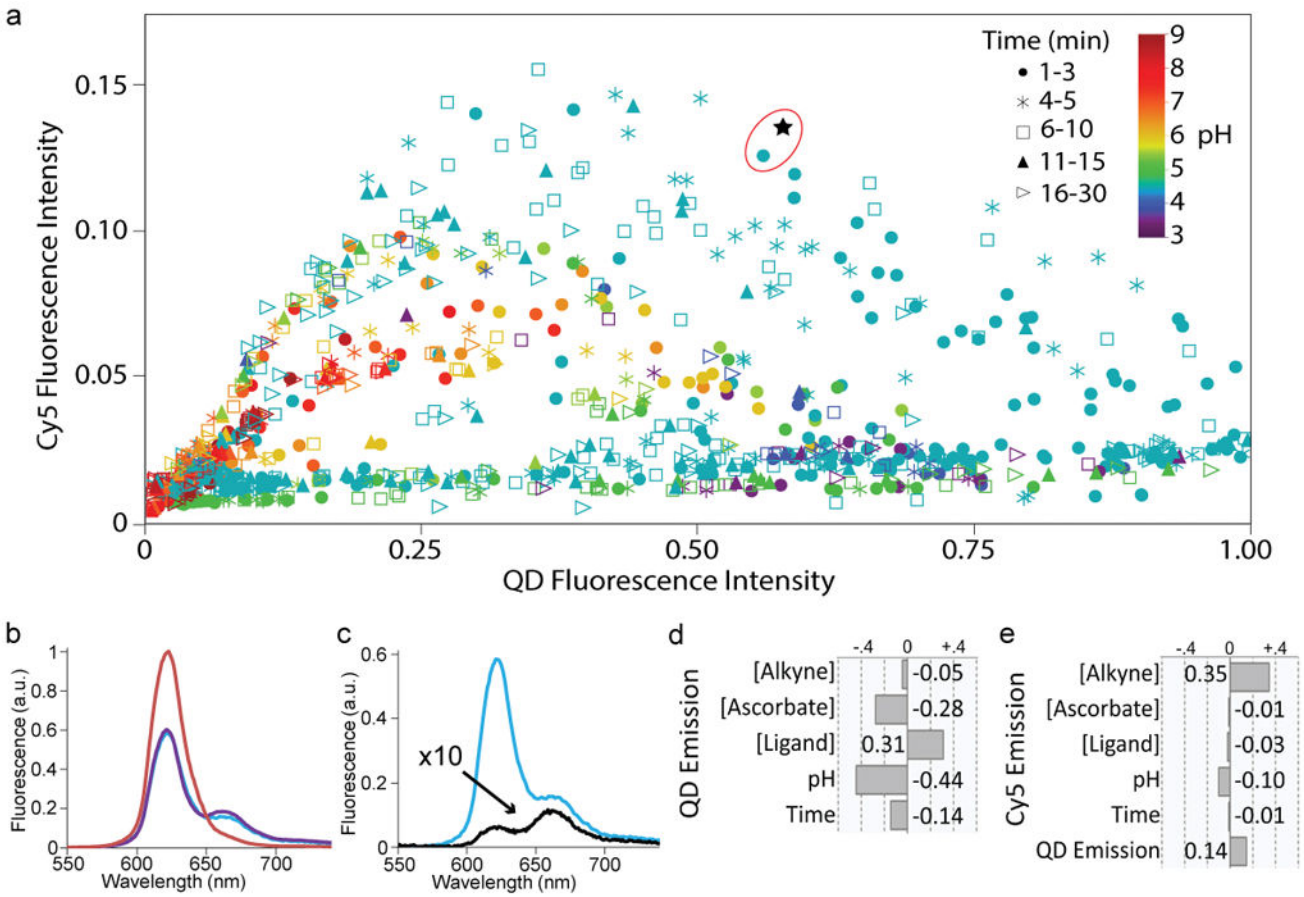

Figure 3.

Combinatorial fluorescence analysis of ~1200 CuAAC reaction conditions for QDs. (a) Integrated Cy5 acceptor emission (670 – 700 nm) *versus* integrated QD emission (600 – 630 nm) for all reaction conditions. Circled data points are fully Cy5-conjugated control (black star) and closest CuAAC conditions (teal circle). (b) Emission spectra of unmodified QDs (red), control Cy5-conjugated QDs (purple), and optimized Cy5 CuAAC-conjugated QDs (teal). (c) Emission spectra of identical Cy5-QD CuAAC reactions with (teal) and without (black, shown magnified 10-fold) THPTA ligands and phosphate-citrate buffer, pH 4.5. (d–e) Pairwise correlations of reaction variables for QD emission (d) and Cy5 emission (e).

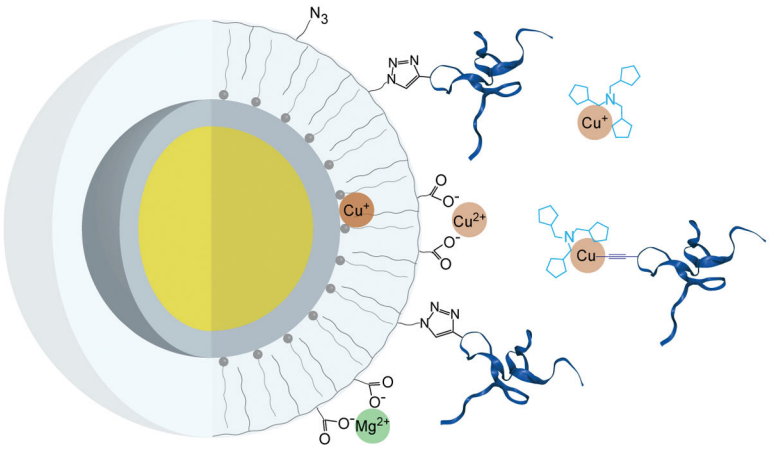

Figure 4.

CuAAC chemistry and Cu quenching mechanisms on amphiphilic polymer-coated QDs. Copper ions may quench QDs by diffusion through the hydrophobic layer to the inorganic crystal or by acting as proximal charge traps when coordinated to surface carboxylates. Peptidyl toxin is shown in dark blue; THPTA ligand in light blue; CdSe core as yellow; and ZnS or CdS shell as gray. Exact structures of Cu-ligand, Cu-QD, and M^{2+}-polymer are unknown.

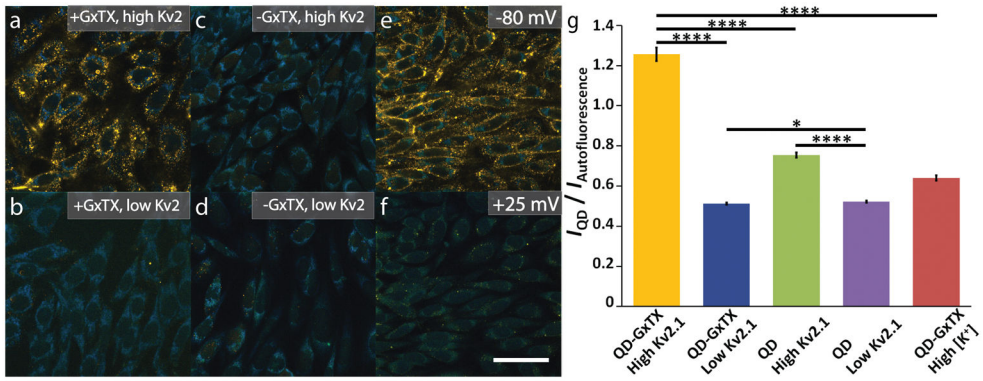

Figure 5.

Live cell imaging of QD-GxTX conjugates on CHO cells expressing Kv2.1 channels. Representative confocal images of QD-GxTX in cells with (a) high and (b) low Kv2.1 channel expression. Yellow is QD emission and blue is cellular autofluorescence. Cells with (c) high and (d) low Kv2.1 expression show similar levels of binding for QDs without conjugated GxTX. Kv2.1-expressing cells stained with QD-GxTX (e) at resting membrane potential and (f) after K^+-induced membrane depolarization. Scale bar is 20 μm. (g) Statistical analysis of emission intensities in (a) – (f) using 560 – 610 nm (QD) and 450 – 500 nm (autofluorescence) integrated emissions. Error bars are standard error. P values: **** ≡ $p < 0.0001$, * ≡ $p < 0.2$ (not significant). $N = 100$ cells.